ORIGINAL RESEARCH

Analysis of Human microRNA Expression Profiling During Diquat-Induced Renal Proximal Tubular Epithelial Cell Injury

Yang Chen[1], Hui-Yi Li[1], Jian-Shu Liu[1], Dao-long Jiang[1], Hao-nan Zheng[2], Xue-Song Dong[1]

[1]Department of Emergency, The First Hospital of China Medical University, Shenyang, 110001, People's Republic of China; [2]No.105 Phase, The First Clinical College of China Medical University, Shenyang, 110001, People's Republic of China

Correspondence: Xue-Song Dong, Department of Emergency, The First Hospital of China Medical University, No. 155 of Nanjing North Street, Heping District, Shenyang, 110001, People's Republic of China, Tel +86 024-26111099; +86 024-83282011, Email dongxunsongdxs0@126.com

Background: We established a diquat-induced human kidney-2 cells (HK-2 cells) apoptosis model in this study to identify differentially expressed microRNAs (miRNAs) and signaling pathways involved in diquat poisoning via gene sequencing and bioinformatics analysis and explored the related therapeutic benefits.

Methods: The effects of diquat on the viability and apoptosis of HK-2 cells were explored using the CCK-8 and Annexin V-FITC/PI double staining methods. Total RNAs were extracted using the TRizol method and detected by Illumina HiSeq 2500. Bioinformatics analysis was performed to explore differentially expressed (DE) miRNAs, their enriched biological processes, pathways, and potential target genes. The RT-qPCR method was used to verify the reliability of the results.

Results: Diquat led to HK-2 cell injury and apoptosis played an important role, hence an HK-2 cell apoptosis model in diquat poisoning was established. Thirty-six DE miRNAs were screened in diquat-treated HK-2 cells. The enriched biological process terms were mainly cell growth, regulation of apoptotic signaling pathway, extrinsic apoptotic signaling pathway, and Ras protein signal transduction. The enriched cellular components were mainly cell-cell junction, cell-substrate junction, ubiquitin ligase complex, and protein kinase complex. The enriched molecular functions were mainly Ras GTPase binding, ubiquitin-like protein transferase activity, DNA-binding transcription factor binding, ubiquitin-protein transferase activity, nucleoside-triphosphatase regulator activity, transcription coactivator activity, and ubiquitin-like protein ligase binding. Signaling pathways such as MAPK, FoxO, Ras, PIK3-Akt, and Wnt were also enriched.

Conclusion: These findings aid in understanding the mechanisms of diquat poisoning and the related pathways, where DE miRNAs serve as targets for gene therapy.

Keywords: apoptosis, biological processes, diquat, HK-2 cells, microRNA

Background

Diquat, whose chemical name is 1,1'-ethyl-2,2'-bipyridiniumion, is a non-selective contact herbicide and desiccant, commonly used in agriculture to control terrestrial and aquatic vegetation.[1,2] More than 20 countries or regions have banned or severely restricted the use of paraquat in recent years.[3,4] Diquat is sold extensively in the herbicide market as a replacement for paraquat. As a result, the number of clinical instances of diquat poisoning has steadily climbed over the past few years. Patients with diquat poisoning have a greater fatality rate because there are no antidotes available. Thus, diquat poisoning remains a major clinical concern.

Kidneys are the most afflicted organs in patients with diquat poisoning, with the proximal renal tubule experiencing the most severe impact and damage.[1] Diquat can be absorbed into the organism by the gastrointestinal tract, skin, and other routes, and the kidney is the primary excretory pathway for this substance.[5,6] Severe diquat poisoning results in multiple organ dysfunction syndromes (MODS), mainly related to the heart, liver, and kidneys, which are associated with high mortality within several hours to a few days.[1,7–10] Patients with diquat poisoning complicated with acute renal injury

4953

have an abysmal prognosis and an increased risk of death, manifesting oliguria, anuria, proteinuria, hematuria, pyuria, azotemia, and acute renal failure.[1,6] In addition, researchers discovered that kidney damage produced by diquat poisoning significantly harmed the renal proximal tubule.[6,11] Thus, research continues into the prevention and treatment of acute renal damage caused by diquat.

Diquat causes cells to produce active substances such as reactive oxygen species (ROS) and reactive nitrogen species (RNS) that can initiate cell apoptosis.[9] The occurrence of apoptosis may be related to activation of nuclear factor kappa-B (NF-κB), damage to mitochondria and DNA, activation of tumor protein p53 (p53), and other factors.[12–15] The process of apoptosis is particularly complex and involved in the regulation of multiple signaling pathways.[16,17] Many factors regulate signaling pathways, and microRNAs (miRNAs) is one of the most common ones. miRNA is a revolutionary, highly conserved non-coding single-stranded small RNA with 18 to 25 nucleotides.[18–20] The vital role of miRNAs in intoxication mechanisms, including bipyridine, diquat, and paraquat poisoning has been well acknowledged.[21–23] However, there is currently insufficient research on diquat-induced miRNA changes in cells or organisms. HK-2 cells have been proven to be a powerful tool to study renal proximal tubule cell apoptosis and injury[24] and were selected to meet the needs and intentions of our study.

Materials and Methods

Reagents and Antibodies

HK-2 cells were derived from Guangzhou Cellcook Biotech Co., Ltd. Diquat was obtained from Sigma-Aldrich Co., Ltd. In addition, phosphate-buffered saline (PBS), fetal bovine serum (FBS), and Dulbecco's modified eagle medium: nutrient mixture F-12 (DMEM/F12) were purchased from Corning, Inc. Annexin V- FITC Apoptosis Detection Kit and Cell Counting Kit-8 (CCK-8) were from Dojindo Molecular Technologies, Inc. TRIzol[TM] Reagent was manufactured by Invitrogen. Taq DNA Polymerase and miRNA first-strand cDNA synthesis were provided by Nanjing Vazyme Biotech Co., Ltd. miRNA primers were synthesized by Sangon Biotech Co., Ltd. Primer U6 was purchased from Genepharma Co., Ltd.

Cell Culture

HK-2 cells were cultured in DMEM/F12 medium with 10% FBS, seeded onto poly-1-lysine-coated plates, and grown at 37 °C in a humidified 5% CO_2 atmosphere, in a cell incubator. Cells used for cell viability assays were grown in 96-well plates, whereas those used for cell apoptosis, microarray, and RT-qPCR were grown in 6-well plates. The cell density was 5×10^4 cells per well for 96-well plates, and 1×10^5 cells per well for 6-well plates, and they were allowed to attach overnight. The medium was changed daily, and cell subculture was performed at 70–80% of the intersection.

Cell Viability Assay

A CCK-8 assay was conducted to determine cell viability. The cells were evenly seeded into a 96-well plate at a density of 5×10^4 cells and 90 μL per well overnight. DMEM/F12, PBS and diquat were used to prepare 200, 400, 600, 800, 1000, and 1200 μmol/L of diquat mixed solution. Then, the diquat preparations were added to a 96-well plate with 10 μL per well for 24 h, and the same amount of PBS was added to the control (CTRL) group. After diquat treatment, 10 μL CCK-8 solution was added to every well for 3 h. An enzyme-labelling instrument measured absorbance at 450 nm.

Cell Apoptosis Assay

The cells were seeded into 6-well culture dishes at a density of 1×10^5 cells per well. The culture media were changed overnight with 3 mL of diquat preparations whose concentrations were 40, 80, and 120 μmol/L and cultured for 24 h, with the same amount of PBS added to the CTRL group. Cells in every well were digested with EDTA-free trypsin and centrifuged, to collect cells. The cells were washed twice with pre-chilled PBS and once with pre-cold 1×buffer. The cells were later resuspended with 100 μL of 1×buffer and 5 μL of Annexin V, as well as 5 μL of PI were added per group for 15 min. Subsequently, every group received 400 μL of 1×buffer and cells were observed using BD FACSAria™ Fusion within 1 h.

RNA Extraction

RNA was extracted with the TRIzol reagent according to the manufacturer's instructions. The experimental groups were treated with 80 μmol/L of diquat, and the CTRL groups were treated with the same amount of PBS and then cultured for 24 h. After discarding the culture medium, 1 mL of Trizol was added for 8 min at room temperature. Subsequently, they were transferred into the RNAse-free EP tube. Next, 200 μL of chloroform were added to the tubes, shaken vigorously for 10s, incubated at room temperature for 2 min, and centrifuged at 12,000 g for 15 min at 4 °C. The water phase was then done in a new EP tube that contained 600 μL isopropanol upside down, mixed well, and incubated at room temperature for 10 min before centrifuging at 12,000 g for 10 min at 4 °C. The supernatant fluid was discarded, 1 mL of 75% ethanol was added, washed once, and centrifuged at 7500 g for 5 min at 4 °C. After aspirating the supernatant fluid, samples were dried at room temperature for 10 min and dissolved in DEPC water. The quality of RNA was determined and stored at −80 °C. Total RNA was extracted from three independent experiments.

miRNA Library Construction and Sequencing

The RNA sequencing was performed by Guangzhou Rubio Biotechnology Co., Ltd. The concentration and quality of RNA was measured using an Agilent Bioanalyzer 2100, and RIN > 7.0 indicated good quality for RNA sequencing. Small purified RNAs were ligated with 3' and 5' adapters. Reverse transcription followed by reverse transcription-quantitative polymerase chain reaction (RT-qPCR) was used to synthesize cDNA. Purified cDNA library products with a size of ~50 base pairs (bp) were subjected to single-end sequencing on an Illumina HiSeq 2500 System. More than 10 million reads (raw data) were generated for each RNA library. We compared raw sequencing data with databases miRbase version 22, Rfam 12.1, and Pirnabank, and then the known ncRNAs were annotated. The clean reads used miRDeep2 software to compare all miRNA mature body sequences of this species in the miRbase. The v22 database was used to obtain the miRNA structure, length, expression, and other pertinent information.

RT-qPCR

Based on the miRNA expression profiles, six of the most apparent changes in miRNAs were chosen for further verification. Reverse transcription reaction conditions were 25 °C for 5 min, 50 °C for 15 min, and 85 °C for 5 min. For pre-denaturation, the PCR program was set at 95 °C for 5 min. For the cycling reaction, 95 °C for 10 sec and 60 °C for 30 sec for 40 cycles were set, and for melt curves, 15 sec at 95 °C, 60 sec at 60 °C, and 15 sec were set at 95 °C. Primer sequences for the six miRNAs used for reverse transcription and PCR are listed in Table 1 and Table 2. In addition, U6 was chosen for miRNA normalization. All the above experiments were conducted according to the manufacturer's instructions.

Table 1 Primer Sequence for Real-Time PCR

ID	Primer Sequence (from 5' to 3')
has-miR-1255b-5p RT	GTCGTATCCAGTGCAGGGTCCGAGGTATTCGCACTGGATACGACAACCAC
has-miR-1255b-5p F	CGCGGCGATGAGCAAAGAAA
has-miR-1910-3p RT	GTCGTATCCAGTGCAGGGTCCGAGGTATTCGCACTGGATACGACTGTCAT
has-miR-1910-3p F	GCGGAGGCAGAAGCAGG
has-miR-1972 RT	GTCGTATCCAGTGCAGGGTCCGAGGTATTCGCACTGGATACGACTGAGCC
has-miR-1972 F	CGTCAGGCCAGGCACAGT
has-miR-2276-3p RT	GTCGTATCCAGTGCAGGGTCCGAGGTATTCGCACTGGATACGACCCTCGC
has-miR-2276-3p F	CGCGTCTGCAAGTGTCAGAG
has-miR-4443 RT	GTCGTATCCAGTGCAGGGTCCGAGGTATTCGCACTGGATACGACAAAACC
has-miR-4443 F	CATAGCGCTTGGAGGCGTG
has-miR-598-5p RT	GTCGTATCCAGTGCAGGGTCCGAGGTATTCGCACTGGATACGACGCTCAC
has-miR-598-5p F	GCGGTGATCCCGATGGT
R	AGTGCAGGGTCCGAGGTATT
U6 F	CGCTTCGGCAGCACATATAC
U6 R	TTCACGAATTTGCGTGTCATC

Table 2 Differentially Expressed miRNAs

Change	miRNA	log2	*p*-value	Change	miRNA	log2	*p*-value
Up	hsa-miR-548z	5.63	0.0052	Down	hsa-miR-26a-1-3p	−1.09	0.0198
	hsa-miR-548h-3p	5.63	0.0052		hsa-miR-6783-3p	−1.11	0.0494
	hsa-miR-1538	5.62	0.0074		hsa-miR-155-3p	−1.23	0.0348
	hsa-miR-5699-3p	5.28	0.0090		hsa-miR-548d-3p	−1.60	0.0368
	hsa-miR-6884-5p	5.22	0.0199		hsa-miR-199b-5p	−1.70	0.0224
	hsa-miR-4449	5.18	0.0269		hsa-miR-6514-5p	−1.83	0.0390
	hsa-miR-6815-5p	5.11	0.0181		hsa-miR-1292-3p	−1.84	0.0221
	hsa-miR-3175	5.05	0.0165		hsa-miR-766-5p	−1.88	0.0159
	hsa-miR-4443	3.00	0.0002		hsa-miR-1972	−2.04	0.0042
	hsa-miR-656-3p	2.73	0.0007		hsa-miR-598-5p	−2.28	0.0009
	hsa-miR-4485-3p	2.35	0.0000		hsa-miR-2276-3p	−2.32	0.0015
	hsa-miR-29a-5p	1.86	0.0375		hsa-miR-3121-3p	−4.68	0.0398
	hsa-miR-195-5p	1.74	0.0073		hsa-miR-6726-3p	−4.68	0.0395
	hsa-miR-6511a-5p	1.67	0.0005		hsa-miR-6806-3p	−5.02	0.0289
	hsa-miR-4508	1.27	0.0414		hsa-miR-6852-5p	−5.13	0.0174
	hsa-miR-1255b-5p	1.16	0.0018		hsa-miR-377-5p	−5.17	0.0207
	hsa-miR-9898	1.02	0.0336		hsa-miR-4456	−5.57	0.0467
	hsa-miR-7704	1.02	0.0000		hsa-miR-1910-3p	−5.62	0.0002

Enrichment Analyses

We predicted downstream target genes of miRNA through four online analysis platforms, TargetScan (http://www.targetscan.org/vert_72/), miRDB (http://mirdb.org/), miRTarBase (https://mirtarbase.cuhk.edu.cn/), and miRWalk (https://mirwalk.umm.uni-heidelberg.de). The prediction results of the miRTarBase or the miRDB, miRWalk, and TargetScan software at the same time were considered as candidate target genes of miRNA. When the two software did not predict the candidate target genes, prediction results of a single database were selected. The functional classification and significant pathways of the differentially expressed miRNA parent genes were performed by Gene Ontology (www.geneontology.org) and Kyoto Encyclopedia of Genes and Genomes (KEGG) database (www.genome.jp/kegg). The analysis results were visualized using the ImageGP (http://www.ehbio.com/ImageGP/index.php/) platform.

miRMA-mRNA Network Analysis

Co-expression networks were constructed using Cytoscape v3.6.1 to intuitively describe pathways and GO analysis results. The screening had to meet with perfect seed-matched sequences between miRNAs and target genes in TargetScan, and a target score ≥ 80 in miRDB. Based on the above prediction results of target genes, a sample diagram of the regulatory network was drawn.

Statistical Analysis

miRNAs with similar expression patterns were clustered using a hierarchical clustering analysis. Differentially expressed miRNAs between samples were selected through two levels of difference factors ($|log2(FoldChange)|>1$) and significance level (P value<0.05). Data for CCK-8, flow cytometry, and qRT-PCR were expressed as the mean ± SD of three or more independent experiments. We used GraphPad Prism 9.0 and SPSS 25.0 software for statistical analysis. Statistical methods such as one-way ANOVA, post-hoc Tukey's test, and paired *t*-test were used for experimental data analysis. Statistical significance was defined as a P value < 0.05.

Results

Diquat Was Cytotoxic to HK-2 Cells

Diquat administration significantly decreased cell viability in the presence of 20–120 μmol/L diquat in a concentration-dependent manner (Figure 1A). Compared to the CTRL group, diquat treatment with 40–120 μmol/L had a more dramatic effect on HK-2 cells ($P < 0.001$). When HK-2 cells were treated with 20 μmol/L diquat, the cell viability was also significantly decreased, but the reduction was lower than that in the high-concentration groups ($P < 0.05$). Moreover, cell viability with diquat at 80 μmol/L was decreased by about 50%, approximating the median inhibitory concentration.

Diquat-Induced HK-2 Cell Apoptosis

We successfully detected the apoptosis rate of HK-2 cells treated with different concentrations of diquat (Figure 1B and C) and noticed that this rate increased in a concentration-dependent manner at 24 h. The apoptosis rate of diquat groups at 80 μmol/L and 120 μmol/L significantly increased compared with that in the CTRL groups, while in the 40 μmol/L groups, the rates varied but were not considered statistically significant ($P < 0.05$). Among them, the apoptosis rate at the half-lethal dose (LD50) was 25.89%. Therefore, it was concluded that cell apoptosis was one of the critical reasons for the decline of cell viability.

Summary of miRNA-Seq Data

Small RNA expression profiles were obtained in HK-2 cells treated with PBS or diquat with a concentration of 80 μmol/L based on the results presented above. A considerable number of small RNAs were identified, and 6,973,030 and 6,942,597 were generated in the CTRL and diquat groups, respectively. Moreover, 76.24% and 73.77% of the total tags in CTRL and diquat groups were retained as clean tags after removing the low-quality tags, contaminants, and ligation products. The length distribution of small RNAs indicates that the size of most small RNAs is 22 nt, which means that miRNA sequences were highly enriched in the library. In all, 754 and 744 miRNAs were identified in the databases mentioned as known miRNAs in the CTRL and diquat groups, respectively, and the remaining unannotated miRNAs were classified as novel miRNAs.

miRNA Profile Analysis

The Pearson correlation coefficient (r) indicated that the correlation between samples was exceptionally high, ranging between 0.992 and 1.000 (Figure 2A). A Venn diagram was constructed using clean data between the CTRL and diquat groups, and 17% of miRNAs showed common differential expression (DE) (Figure 2B). Principal component analysis
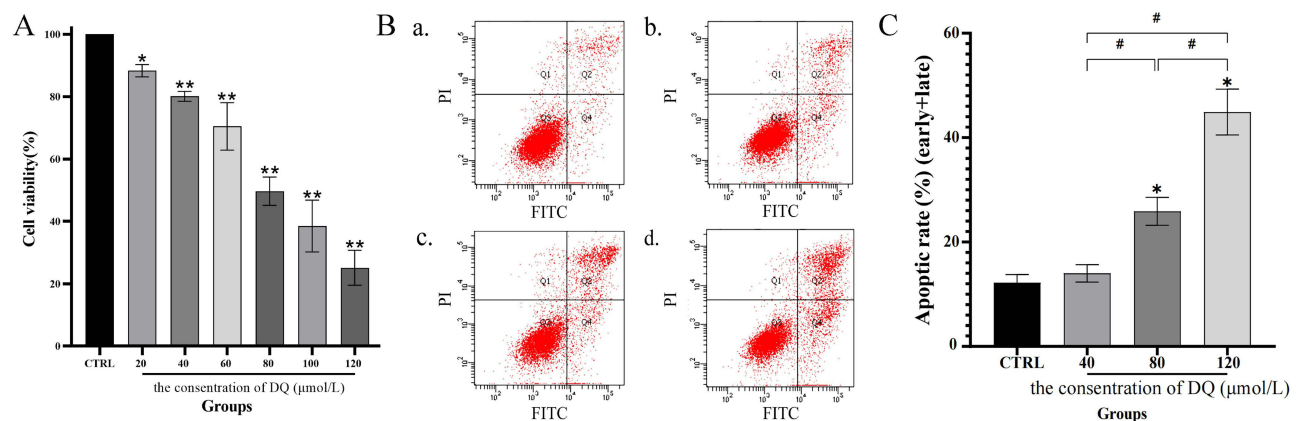

Figure 1 HK-2 cell cytotoxicity and apoptosis induced by diquat.
Notes: (**A**) Cell viability. HK-2 cells were cultured in a cell medium with diquat (0, 20, 40, 60, 80, 100, and 120 μmol/L) for 24 h, and cell viability was measured by CCK-8 assay. (**B** and **C**) Cell apoptosis rate. HK-2 cells were cultured in a cell medium with diquat (0, 40, 80, and 120 μmol/L) for 24 h. Flow cytometry was used to detect the apoptosis rate of HK-2 cells by double staining of Annexin V and PI. Data is presented as mean ± SD of three or more independent experiments, *$P<0.05$ and **$P<0.001$ with respect to the CTRL group, and #$P<0.05$ with respect to the diquat group, indicating statistical significance by one-way ANOVA and post-hoc Tukey's test.
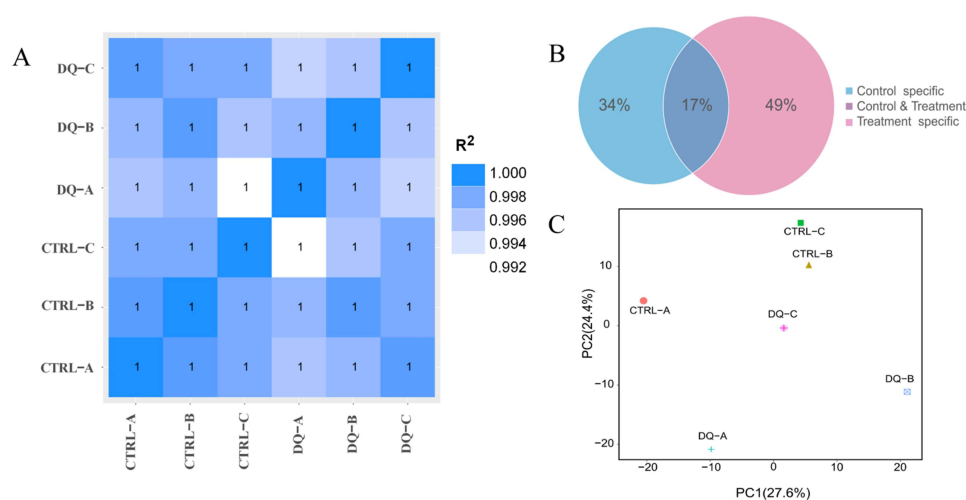
Figure 2 Inter-sample correlation, principal components, and public and unique sequence analysis.
Notes: (**A**) Correlation coefficient plot between samples. (**B**) The plot of the ratio analysis of shared and unique sequences between samples. (**C**) A principal component analysis algorithm used to analyze the samples.

(PCA) of the log2 gene expression data showed that the diquat group differed from the CTRL group (Figure 2C). Thirty-six DE miRNAs in the diquat group, including 18 up-regulated and 18 down-regulated ones were comparable with the CTRL group (Table 2). After clustering the columns (samples) and rows (miRNAs), the heat map displayed the clustering results of samples and miRNAs in a single graph (Figure 3A–C). The intensity of changes in miRNA expression was indicated in different colors. These DE miRNAs clearly distinguished the CTRL group from the diquat group.

Verification of Transcriptomic Analysis with qRT-PCR

The expression levels of six candidate miRNAs selected randomly from the library were determined with qRT-PCR to validate the results. The expression of hsa-miR-1910-3p, hsa-miR-1972, and hsa-miR-598-5p in the diquat group decreased more than in the CTRL group, and the expression of hsa-miR-1255b-5p and hsa-miR-4443 in the diquat group increased considerably (Figure 3D) ($P < 0.05$). The results of the qRT-PCR experiments showed that the expression levels of these miRNAs were almost identical to those indicated by the miRNA-seq data.

GO and KEGG Pathway Analysis

The DE miRNAs were further investigated, and the 16,759 of their target genes were predicted. To further analyze their functions, GO and KEGG pathways were subsequently implemented. The analyses revealed that there were 6445 biological processes (BP), 760 cellular components (CC), and 1188 molecular functions (MF). Furthermore, the enriched BP terms were mainly cell morphogenesis regulation, regulation of GTPase activity, cell growth, histone modification, Ras protein signal transduction, regulation of apoptotic signaling pathway, activation of protein kinase activity, protein autophosphorylation, extrinsic apoptotic signaling pathway, and regulation of extrinsic apoptotic signaling pathway (Figure 4A). The enriched CC terms were nuclear envelope, transcription factor complex, cell-cell junction, cell-substrate junction, transport vesicle, nuclear membrane, ubiquitin ligase complex, and protein kinase complex (Figure 4B). The enriched MF terms were mainly DNA-binding transcription activator activity, RNA polymerase II-specific, protein serine/threonine kinase activity, Ras GTPase binding, ubiquitin-like protein transferase activity, DNA-binding transcription factor binding, ubiquitin-protein transferase activity, nucleoside-triphosphatase regulator activity, transcription coactivator activity, and ubiquitin-like protein ligase binding (Figure 4C). In addition, the enriched KEGG pathways included the mitogen-activated protein kinase (MAPK) signaling pathway, forkhead box O (FoxO) signaling pathway, Ras signaling pathway, phosphatidylinositide 3-kinases (PI3K)- protein kinase B (Akt) signaling pathway, Wingless / Integrated (Wnt) signaling pathway, and apoptosis-multiple species (Figure 4D).
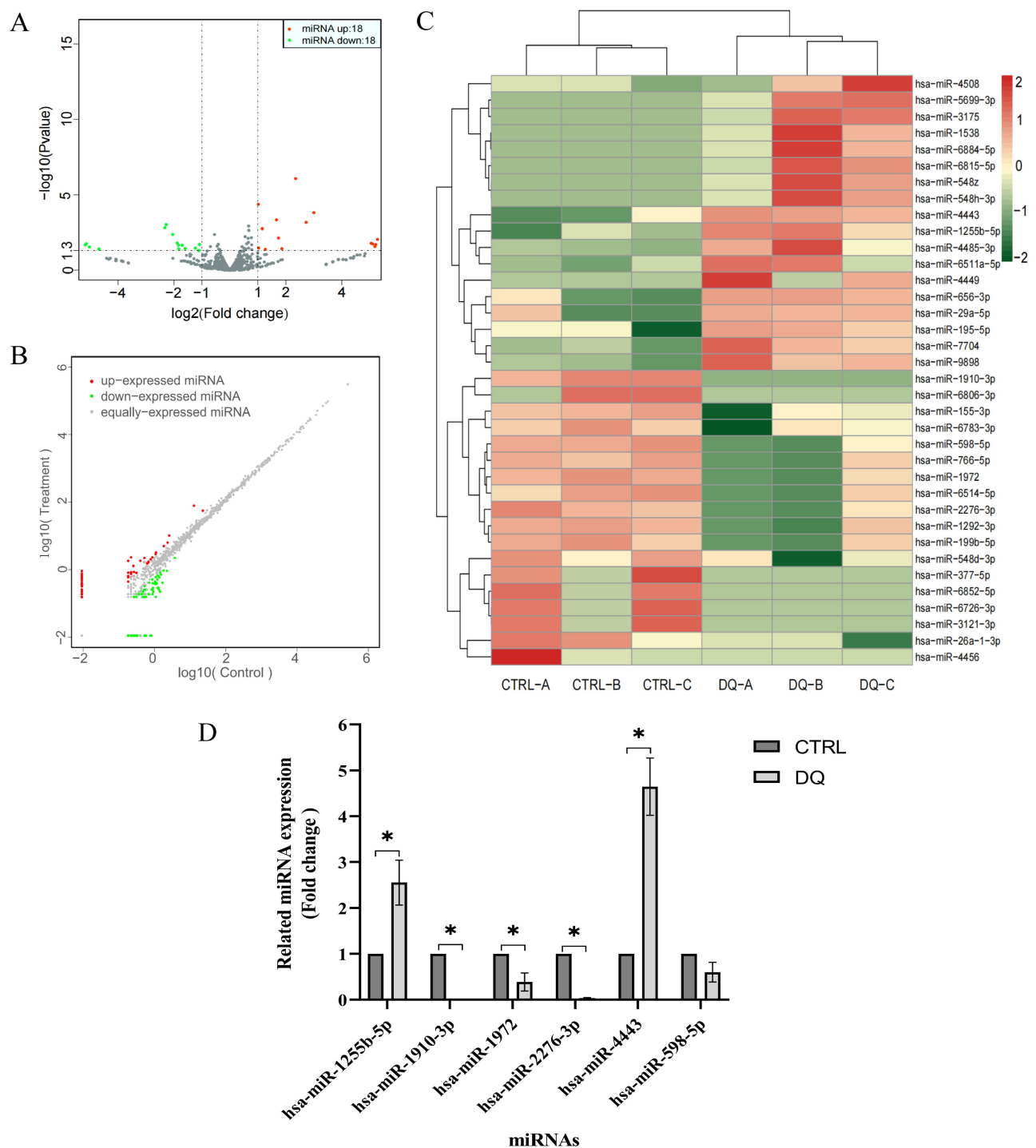
Figure 3 Profiles of the DE miRNAs. HK-2 cells were cultured in a medium containing 80 μmol/L diquat or an equivalent amount of PBS for 24 h.
Notes: (**A**) Volcano plot of miRNAs. (**B**) Scatter plot of differences in miRNAs between samples. (**C**) Heat map of DE miRNAs in HK-2 cells. |log2(FoldChange)| > 1, P value <0.05 relative to the CTRL group. (**D**) Histogram of RT-qPCR results. U6 normalized miRNA expression. Values are expressed as the mean ± SD, with *P value <0.05, diquat treatment group vs CTRL group.

miRNA-mRNA Network Analysis

It has been previously identified that the gene expression, post-transcriptionally regulated by miRNAs is widely distributed (Figure 5). As shown in Figure 5, genes, including caspase-8 (CASP8), CASP10, CASP3, CASP7, P53, Fas cell surface death receptor (FAS), tumor necrosis factor (TNF), B-cell lymphoma-2 (BCL-2), BCL2-associated
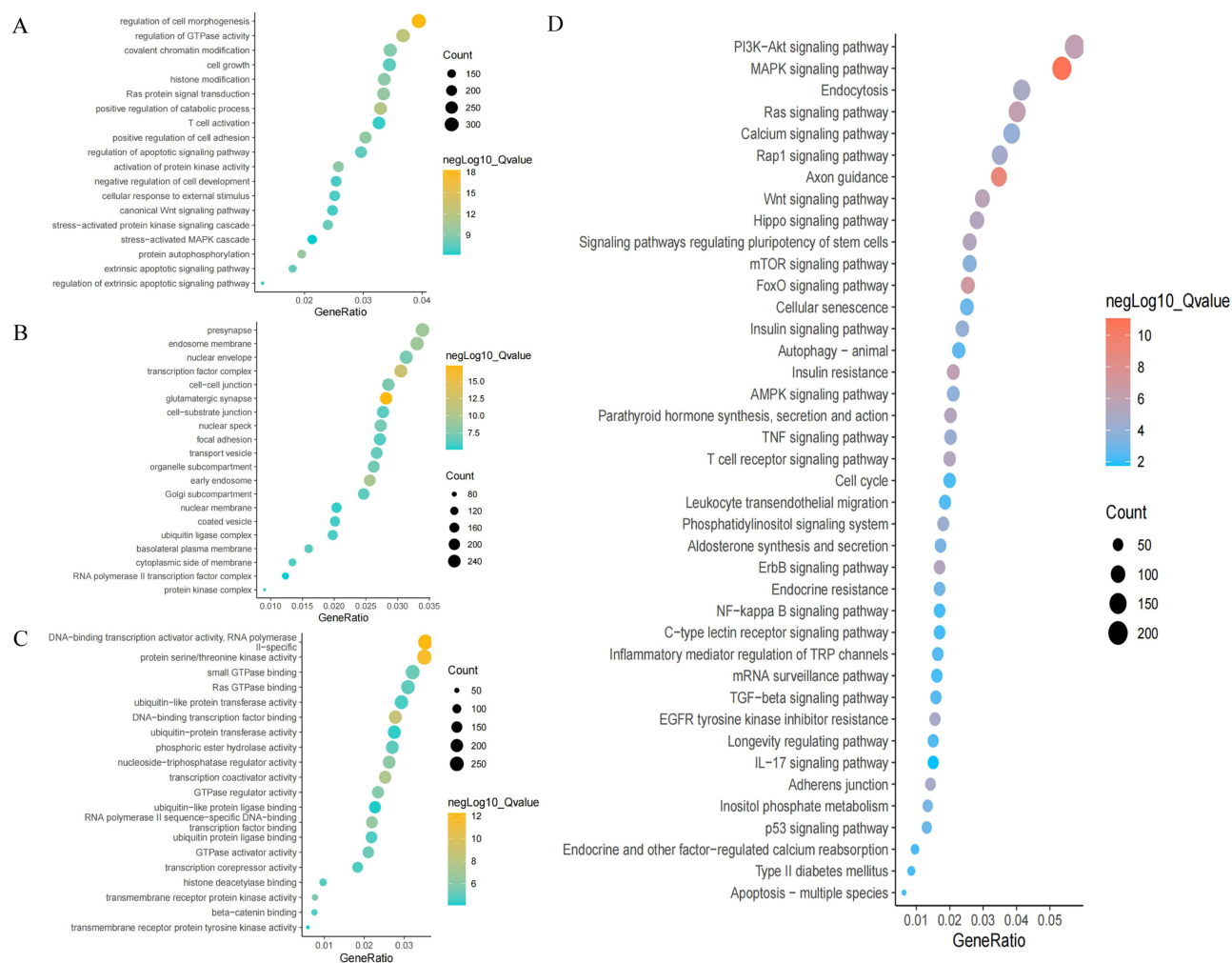
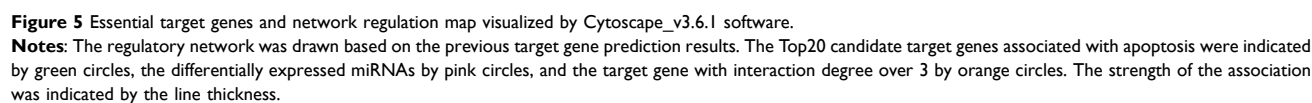**Figure 4** Results of GO and KEGG analyses visualized by imageGP platform.
Notes: (**A–C**) Enrichment plot of GO analysis. (**D**) Pathway analysis enrichment plot for KEGG. *Q*-value < 0.05.

X (BAX), ubiquitin protein ligase E3A (UBE3A), ubiquitin-conjugating enzyme E2 Z (UBE2Z), ubiquitin-conjugating enzyme E2 K (UBE2K), ubiquitin-conjugating enzyme E2 D3 (EBE2D3), ubiquitin-conjugating Enzyme E2 D1 (UBE2D1), and ubiquitin-conjugating Enzyme E2 K (UBE2K) were targeted by these DE MiRNAs. A miRNA can recognize multiple target genes at the same time, and multiple miRNAs can also regulate a gene.

Discussion

Diquat has been reported to be toxic to humans and animals and the damage caused by its toxic effects can be roughly classified into the following two types:[1,25,26] First, diquat produces direct contact burns in humans and animals, resulting in tissue necrosis, mucosal erosion, or hemorrhage.[1,26,27] Secondly, it also activates a reduction-oxidative process that generates ROS and RNS in cells, leading to oxidative stress, which in turn leads to cellular dysfunction.[1,26] It was previously found that diquat-induced superoxide damages mitochondria and endoplasmic reticulum, initiates autophagy, and induces apoptosis.[13,28] In this study, we found that diquat reduced the viability of HK-2 cells, and that apoptosis is triggered by HK-2 cell damage.

In this study, 18 miRNAs species, including hsa-miR-1910-3p, hsa-miR-1972, and hsa-miR-598-5p, were down-regulated, while18 miRNAs species, including hsa-miR-1255b-5p and hsa-miR-4443, were upregulated. Existing studies have found that miRNAs play a significant role in various biological processes, including cell apoptosis.[29,30] Furthermore, miRNAs have diagnostic and therapeutic value in many fields, such as tumor suppression, inflammation,

Figure 5 Essential target genes and network regulation map visualized by Cytoscape_v3.6.1 software.
Notes: The regulatory network was drawn based on the previous target gene prediction results. The Top20 candidate target genes associated with apoptosis were indicated by green circles, the differentially expressed miRNAs by pink circles, and the target gene with interaction degree over 3 by orange circles. The strength of the association was indicated by the line thickness.

and poisoning.[30,31] For example, in prostate cancer cells, miR-1972 targeted the miRNAs LIM and SH3 protein 1 (LASP1) and negatively regulated its expression, while upregulating miR-1972 inhibited cell proliferation, migration, invasion, and tumor formation and enhanced apoptosis.[32] In stroke-induced immunodeficiency syndrome, the increased expression of miR-4443 induced monocyte dysfunction by targeting tumor necrosis factor receptor-associated factor 4 (TRAF4), which may function as a crucial mediator, but in Graves' disease, this process induces CD4+ T cell dysfunction by targeting TRAF4.[33,34] Besides, in mammary epithelial cells during breast cancer, miR-1910-3p promotes proliferation and migration, inhibits apoptosis, and induces autophagy.[29] Therefore, it is reasonable to believe that these DE miRNAs are vital in HK-2 cell apoptosis induced by diquat.

Further analysis revealed that these GO terms and KEGG pathways were not specific to nephrocytes, indicating that the toxicity of diquat can affect cells of multiple organs. The analysis also revealed that the HK-2 cell apoptosis induced by diquat was mainly mediated through the exogenous apoptosis signaling pathway. Previous studies proved that exogenous apoptosis signaling pathways were triggered by ligand binding to transmembrane receptors, such as tumor necrosis factor receptor 1 (TNFR1) and Fas receptor (FasR).[35,36] CASP8 and CASP10 were verified to initiate death receptor-mediated exogenous apoptosis.[37,38] Three signaling pathways, namely, FAS, TNFR1, and TRAIL, are currently the main exogenous death receptor pathways, among which the FAS-mediated apoptosis conduction pathway is the most

classical.[35,39,40] FAS binds to the death ligand to recruit pro-CASP8 and form a death-induced signaling complex (DISC), and pro-CASP8 in DISC self-cleaves into active CASP8.[41] As an initiator caspase, CASP8 is able to activate the downstream caspase family members of the entire cell apoptosis transduction pathway.[42] The DE miRNAs in this study can target CASP8 and CASP10 that are at the beginning of the apoptosis conduction pathway, and activate the downstream CASPs, like CASP3 and CASP7.[41,43] Both the primed CASP8 and CASP10, and CASP7 and CASP3 were the candidate target genes for the differentially expressed RNAs identified in this study—hsa-miR-6884-5p, hsa-miR-1972, and hsa-miR-377-5p targeted CASP8, hsa-miR-26a-1-3p targeted CASP10, and hsa-miR-6806-3p targeted CASP3. Therefore, FAS and CASP play an important role in HK-2 cell apoptosis induced by diquat, mainly through the exogenous apoptosis signaling pathway. Besides, the role of the Bcl-2 and TNF family in apoptosis has been known for some time.[35,44] In this study, we found that multiple DE miRNAs could modulate the expression of Bcl-2, BAK1, and TNF, including hsa-miR-195-5p, hsa-miR-4443, and hsa-miR-3121-3p.

Ubiquitination is a kind of protein modification, and we found that molecular functions such as ubiquitin-like protein transferase activity, ubiquitin protein transferase activity, ubiquitin-like protein ligase binding, and ubiquitin-protein ligase binding are enriched. This suggests that the ubiquitination modification of proteins may play an important role when diquat induces apoptosis in HK-2 cells. The major ubiquitin molecules include UBE2D1, UBE2D3, UBE2I, UBE2K, UBE2Z, and UBE3A. Ubiquitination refers to the process in which ubiquitin covalently binds to target proteins when catalyzed by a series of enzymes, basically three enzymes that cooperate during the ubiquitination cascade: E1 ubiquitin activator, E2 ubiquitin-conjugated enzyme, and E3 ubiquitin ligase.[45] Existing studies show that ubiquitination can affect the localization, metabolism, function, regulation, and degradation of proteins and participate in the regulation of almost all life activities, such as cell cycle, proliferation, apoptosis, differentiation, metastasis, gene expression, transcription regulation, signaling, damage repair, and inflammatory immunity.[46,47] As per this study, it is evident that when diquat induces apoptosis in HK-2 cells, multiple miRNAs function by targeting the expression of genes involved in the ubiquitination modification. Several miRNAs such as hsa-miR-29a-5p, hsa-miR-548d-3p, hsa-miR-766-5p, and hsa-miR-3121-3p regulated the ubiquitination process, and most of these DE target genes were associated with E2 ubiquitinates.

This study with both in vitro cell research and data analysis is more reliable than monotonic data analysis. However, experiments with in vitro cells cannot wholly replace in vivo studies. In addition, there are numerous cells in the kidney, with the renal proximal tubule cells being the most prominent and associated with renal damage induced by diquat; hence, they do represent all kidney cells. Different concentrations of diquat may also have unknown effects on the various forms of cell damage. Furthermore, diquat-induced damage to renal proximal tubules as well as the mechanism of action between miRNAs and multiple target genes and pathways are highly complex. Based on our study, we found that miRNAs comprehensively participated in the process of diquat-induced HK-2 cell injury. However, we only investigated a few aspects of the process and did not investigate the involvement of a specific miRNA in the process of diquat-induced HK-2 cell injury in depth. Future study is required to confirm this aspect.

Conclusion

Diquat poisoning remains a challenging problem in emergency and critical care medicine as it has no specific antidote. In this study, the toxic mechanism of diquat-induced damage to HK-2 cells was preliminarily explored, and it was found that diquat had toxic effects that could lead to the apoptosis of HK-2 cells. In addition, miRNAs such as hsa-miR-1910-3p, hsa-miR-1972, and hsa-miR-598-5p in HK-2 cells decreased after diquat treatment, while hsa-miR-1255b-5p and hsa-miR-4443 increased. Furthermore, GO and KEEG analysis revealed that these DE miRNAs were enriched in biological processes and signaling pathways that were involved in apoptosis. These DE miRNAs could target genes such as CASP8, FAS, BAX, and BCL2 and play a role in apoptosis and ubiquitination. Overall, in this study we explored the unique expression pattern of miRNAs during diquat-induced HK-2 cell injury, which provides a theoretical basis for future research on the pathogenesis of diquat-induced renal injury and may shed light on potential therapeutic targets.

Abbreviations

MODS, multiple organ dysfunction syndromes; ROS, reactive oxygen species; RNS, reactive nitrogen species; NF-κB, nuclear factor kappa-B; p53, tumor protein p53; miRNAs, microRNAs; PBS, phosphate-buffered saline; FBS, fetal bovine serum; CCK-8, Cell Counting Kit-8; RT-qPCR, reverse transcription-quantitative polymerase chain reaction; bp, base pairs; DE, differential expression; PCA, Principal component analysis; BP, biological processes; CC, cellular components; MF, molecular functions; MAPK, mitogen-activated protein kinase; FoxO, forkhead box O; PI3K, phosphatidylinositide 3-kinases; Wnt, Wingless / Integrated; TNF, tumor necrosis factor; BCL-2, cell lymphoma-2; BAX, BCL2-associated X; UBE3A, ubiquitin protein ligase E3A; UBE2Z, ubiquitin-conjugating enzyme E2 Z; EBE2D3, ubiquitin-conjugating enzyme E2 D3; UBE2K, ubiquitin-conjugating Enzyme E2 K.

Data Sharing Statement

The datasets used and/or analysed during the current study available from the corresponding author on reasonable request.

Disclosure

None of the authors have any financial disclosure or conflicts of interest.

References

1. Magalhães N, Carvalho F, Dinis-Oliveira RJ. Human and experimental toxicology of diquat poisoning: toxicokinetics, mechanisms of toxicity, clinical features, and treatment. *Hum Exp Toxicol*. 2018;37(11):1131–1160. doi:10.1177/0960327118765330
2. Oreopoulos DG, McEvoy J. Diquat poisoning. *Postgrad Med J*. 1969;45(527):635–637. doi:10.1136/pgmj.45.527.635
3. Tsen CM, Yu CW, Chuang WC, et al. A simple approach for the ultrasensitive detection of paraquat residue in adzuki beans by surface-enhanced Raman scattering. *Analyst*. 2019;144(2):426–438. doi:10.1039/C8AN01845F
4. Wang X, Wang X, Zhu Y, et al. ADME/T-based strategies for paraquat detoxification: transporters and enzymes. *Environ Pollut*. 2021;291:118137. doi:10.1016/j.envpol.2021.118137
5. Yu G, Cui S, Jian T, et al. Diquat poisoning in a pregnant woman resulting in a miscarriage and maternal death. *Clin Toxicol*. 2021;59(12):1275–1277. doi:10.1080/15563650.2021.1905164
6. Rogers LK, Bates CM, Welty SE, et al. Diquat induces renal proximal tubule injury in glutathione reductase-deficient mice. *Toxicol Appl Pharmacol*. 2006;217(3):289–298. doi:10.1016/j.taap.2006.08.012
7. Lock A. The effect of paraquat and diquat on renal function in the rat. *Toxicol Appl Pharmacol*. 1979;48:321–336. doi:10.1016/0041-008X(79)90039-5
8. Chen Y, Chen Y, Zhang H, et al. Pterostilbene as a protective antioxidant attenuates diquat-induced liver injury and oxidative stress in 21-day-old broiler chickens. *Poult Sci*. 2020;99(6):3158–3167. doi:10.1016/j.psj.2020.01.021
9. Jones GM, Vale JA. Mechanisms of toxicity, clinical features, and management of diquat poisoning: a review. *J Toxicol Clin Toxicol*. 2000;38(2):123–128. doi:10.1081/CLT-100100926
10. Vanholder R, Colardyn F, De Reuck J, et al. Diquat intoxication. *Am J Med*. 1981;70(6):1267–1271. doi:10.1016/0002-9343(81)90836-6
11. Huang Y, Zhang R, Meng M, et al. High-dose diquat poisoning: a case report. *J Int Med Res*. 2021;49(6):1–10. doi:10.1177/03000605211026117
12. Nisar R, Hanson PS, He L, et al. Diquat causes caspase-independent cell death in SH-SY5Y cells by production of ROS independently of mitochondria. *Arch Toxicol*. 2015;89(10):1811–1825. doi:10.1007/s00204-015-1453-5
13. Park A, Koh HC. NF-kappaB/mTOR-mediated autophagy can regulate diquat-induced apoptosis. *Arch Toxicol*. 2019;93(5):1239–1253. doi:10.1007/s00204-019-02424-7
14. Choi SE, Park YS, Koh HC. NF-kappaB/p53-activated inflammatory response involves in diquat-induced mitochondrial dysfunction and apoptosis. *Environ Toxicol*. 2018;33(10):1005–1018. doi:10.1002/tox.22552
15. Gupta S, Silveira DA, Mombach JCM. Towards DNA-damage induced autophagy: a Boolean model of p53-induced cell fate mechanisms. *DNA Repair*. 2020;96:102971. doi:10.1016/j.dnarep.2020.102971
16. Huang J, Liu W, Doycheva DM, et al. Ghrelin attenuates oxidative stress and neuronal apoptosis via GHSR-1alpha/AMPK/Sirt1/PGC-1alpha/UCP2 pathway in a rat model of neonatal HIE. *Free Radic Biol Med*. 2019;141:322–337. doi:10.1016/j.freeradbiomed.2019.07.001

17. Jahan N, Chowdhury A, Li T, et al. Neferine improves oxidative stress and apoptosis in benign prostate hyperplasia via Nrf2-ARE pathway. *Redox Rep*. 2021;26(1):1–9. doi:10.1080/13510002.2021.1871814

18. Bartel DP. MicroRNAs: genomics, biogenesis, mechanism, and function. *Cell*. 2004;116:281–297. doi:10.1016/S0092-8674(04)00045-5

19. Michlewski G, Cáceres JF. Post-transcriptional control of miRNA biogenesis. *RNA*. 2019;25(1):1–16. doi:10.1261/rna.068692.118

20. Han S, Lin F, Ruan Y, et al. miR-132-3p promotes the cisplatin-induced apoptosis and inflammatory response of renal tubular epithelial cells by targeting SIRT1 via the NF-kappaB pathway. *Int Immunopharmacol*. 2021;99:108022. doi:10.1016/j.intimp.2021.108022

21. Jing H, Zhang Q, Li S, et al. Pb exposure triggers MAPK-dependent inflammation by activating oxidative stress and miRNA-155 expression in carp head kidney. *Fish Shellfish Immunol*. 2020;106:219–227. doi:10.1016/j.fsi.2020.08.015

22. Wu J, Zheng C, Wang Y, et al. LncRNA APCDD1L-AS1 induces icotinib resistance by inhibition of EGFR autophagic degradation via the miR-1322/miR-1972/miR-324-3p-SIRT5 axis in lung adenocarcinoma. *Biomark Res*. 2021;9(1):9. doi:10.1186/s40364-021-00262-3

23. Zhan Y, Guo Z, Zheng F, et al. Reactive oxygen species regulate miR-17-5p expression via DNA methylation in paraquat-induced nerve cell damage. *Environ Toxicol*. 2020;35(12):1364–1373. doi:10.1002/tox.23001

24. Ryan MJ, Johnson G, Kirk J, et al. HK-2: an immortalized proximal tubule epithelial cell line from normal adult human kidney. *Kidney Int*. 1994;45:48–57. doi:10.1038/ki.1994.6

25. Zhang JQ, Gao BW, Wang J, et al. Chronic exposure to diquat causes reproductive toxicity in female mice. *PLoS One*. 2016;11(1):e0147075. doi:10.1371/journal.pone.0147075

26. Chen J, Su Y, Lin R, et al. Effects of acute diquat poisoning on liver mitochondrial apoptosis and autophagy in ducks. *Front Vet Sci*. 2021;8:727–766. doi:10.3389/fvets.2021.727766

27. Hao L, Cheng Y, Su W, et al. Pediococcus pentosaceus ZJUAF-4 relieves oxidative stress and restores the gut microbiota in diquat-induced intestinal injury. *Appl Microbiol Biotechnol*. 2021;105(4):1657–1668. doi:10.1007/s00253-021-11111-6

28. Liang H, Ran Q, Jang YC, et al. Glutathione peroxidase 4 differentially regulates the release of apoptogenic proteins from mitochondria. *Free Radic Biol Med*. 2009;47(3):312–320. doi:10.1016/j.freeradbiomed.2009.05.012

29. Wang B, Mao JH, Wang BY, et al. Exosomal miR-1910-3p promotes proliferation, metastasis, and autophagy of breast cancer cells by targeting MTMR3 and activating the NF-kappaB signaling pathway. *Cancer Lett*. 2020;489:87–99. doi:10.1016/j.canlet.2020.05.038

30. Lu Q, Wu R, Zhao M, et al. miRNAs as therapeutic targets in inflammatory disease. *Trends Pharmacol Sci*. 2019;40(11):853–865. doi:10.1016/j.tips.2019.09.007

31. Liu F, Zhang Q, Liang Y. MicroRNA-598 acts as an inhibitor in retinoblastoma through targeting E2F1 and regulating AKT pathway. *J Cell Biochem*. 2020;121(3):2294–2302. doi:10.1002/jcb.29453

32. Wang S, Qiu J, Wang L, et al. Long non-coding RNA LINC01207 promotes prostate cancer progression by downregulating microRNA-1972 and upregulating LIM and SH3 protein 1. *IUBMB Life*. 2020;72(9):1960–1975. doi:10.1002/iub.2327

33. Li S, Lu G, Wang D, et al. MicroRNA-4443 regulates monocyte activation by targeting tumor necrosis factor receptor associated factor 4 in stroke-induced immunosuppression. *Eur J Neurol*. 2020;27(8):1625–1637. doi:10.1111/ene.14282

34. Qi Y, Zhou Y, Chen X, et al. MicroRNA-4443 causes CD4+ T cells dysfunction by targeting TNFR-associated factor 4 in graves' disease. *Front Immunol*. 2017;8:1440. doi:10.3389/fimmu.2017.01440

35. Zhang C, Wang C, Tang S, et al. TNFR1/TNF-α and mitochondria interrelated signaling pathway mediates quinocetone-induced apoptosis in HepG2 cells. *Food Chem Toxicol*. 2013;62:825–838. doi:10.1016/j.fct.2013.10.022

36. Strasser A, Jost PJ, Nagata S. The many roles of FAS receptor signaling in the immune system. *Immunity*. 2009;30(2):180–192. doi:10.1016/j.immuni.2009.01.001

37. Li X, Li F, Zhang X, et al. Caspase-8 auto-cleavage regulates programmed cell death and collaborates with RIPK3/MLKL to prevent lymphopenia. *Cell Death Differ*. 2022;29(8):1500–1512. doi:10.1038/s41418-022-00938-9

38. Miano M, Cappelli E, Pezzulla A, et al. FAS-mediated apoptosis impairment in patients with Alps/Alps-like phenotype carrying variants on CASP10 gene. *Br J Haematol*. 2019;187(4):502–508. doi:10.1111/bjh.16098

39. McGrath EE, Marriott HM, Lawrie A, et al. TNF-related apoptosis-inducing ligand (TRAIL) regulates inflammatory neutrophil apoptosis and enhances resolution of inflammation. *J Leukoc Biol*. 2011;90(5):855–865. doi:10.1189/jlb.0211062

40. Tan S, Liu X, Chen L, et al. Fas/FasL mediates NF-κBp65/PUMA-modulated hepatocytes apoptosis via autophagy to drive liver fibrosis. *Cell Death Dis*. 2021;12(5):474. doi:10.1038/s41419-021-03749-x

41. Liao X, Wang X, Gu Y, et al. Involvement of death receptor signaling in mechanical stretch-induced cardiomyocyte apoptosis. *Life Sci*. 2005;77(2):160–174. doi:10.1016/j.lfs.2004.11.029

42. Fritsch M, Günther SD, Schwarzer R, et al. Caspase-8 is the molecular switch for apoptosis, necroptosis and pyroptosis. *Nature*. 2019;575(7784):683–687. doi:10.1038/s41586-019-1770-6

43. Saggioro FP, Neder L, Stávale JN, et al. Fas, FasL, and cleaved caspases 8 and 3 in glioblastomas: a tissue microarray-based study. *Pathol Res Pract*. 2014;210(5):267–273. doi:10.1016/j.prp.2013.12.012

44. Gu L, Surolia R, Larson-Casey JL, et al. Targeting Cpt1a-Bcl-2 interaction modulates apoptosis resistance and fibrotic remodeling. *Cell Death Differ*. 2022;29(1):118–132. doi:10.1038/s41418-021-00840-w

45. Hu H, Sun SC. Ubiquitin signaling in immune responses. *Cell Res*. 2016;26(4):457–483. doi:10.1038/cr.2016.40

46. Cruz Walma DA, Chen Z, Bullock AN, et al. Ubiquitin ligases: guardians of mammalian development. *Nat Rev Mol Cell Biol*. 2022;23(5):350–367. doi:10.1038/s41580-021-00448-5

47. Narayanan S, Cai CY, Assaraf YG, et al. Targeting the ubiquitin-proteasome pathway to overcome anti-cancer drug resistance. *Drug Resist Updat*. 2020;48:100663. doi:10.1016/j.drup.2019.100663